17th World Conference on Earthquake Engineering, 17WCEE
Sendai, Japan - September 27th to October 2nd, 2021

BROADBAND MICROTREMOR ARRAY EXPLORATION IN KATHMANDU VALLEY, NEPAL

T. Yokoi [1], T. Hayashida [2], M. Bhattarai [3], T. Pokharel [4], S. Shrestha [5], C. Timsina [6], S. Bhattarai [7], R. Sharma [8], D. Nepali [9]

[1] *Senior Fellow, IISEE, Building Research Institute, Japan, tyokoi@kenken.go.jp,*
[2] *Senior Research Scientist, IISEE, Building Research Institute, takumi-h@kenken.go.jp,*
[3] *Seismologist, NEMRC, DMG, Nepal, mb2058@yahoo.com,*
[4] *Geologist, DMG, Nepal, tara_geo@yahoo.com,*
[5] *Senior Divisional Geologist, DMG, Nepal, suresh-shrestha@hotmail.com,*
[6] *Seismologist, NEMRC, DMG, Nepal, chintan1119@gmail.com,*
[7] *Geologist, DMG, Nepal, sunitabhtry.828@gmail.com,*
[8] *Technical Assistant, Seismological Center Surkhet, DMG, Nepal, sendmerajesh2017@gmail.com.*
[9] *Superintendent Geologist, DMG, Nepal, d_nepali@hotmail.com.*

Abstract

Strong ground motion of long duration and long predominant period around 4 s were observed during the 2015 Gorkha earthquake at the central part of the Kathmandu Valley (KTV), Nepal [1],[2], that is a tectonic basin formed during the Himalayan orogeny due to the collision of the Indian plate to the Eurasian plate [3]. The research group to which the authors belong (Group3, SATREPS) has conducted the deep exploration from Dec. 2016 to May 2019 with the aim to reveal the cause of the mentioned phenomena to make use it for the seismic hazard assessment.

We conducted the field observation of microtremor in KTV using 4 broadband seismographs to estimate the shear wave velocity structure of deep sediments. We used also short period seismometers, land geophones and multi-channel data logger for shallow exploration [4]. Due to the difficulty to form a large regular polygon arrays in the densely built-up city, we had to deploy large irregular quadrilateral ones based on the confirmation of the isotropic nature of coherence function of microtremor, whereas equilateral triangular ones for middle and small sizes. The maximum inter-station distances of each sites were about 900m, and 1,400 m at maximum. Recording duration was one night or longer per deployment. Then we applied 2ST-SPAC analysis to these arrays in a combined way to estimate the dispersion curves.

To fix the problem supposed to be caused by the insufficient power of microtremor in the frequency range lower than 0.2 Hz, we have combined the phase velocity of Rayleigh waves that was determined using surface waves components of tectonic earthquake records in the frequency range from 0.03 Hz to 0.13 Hz [5]. For high frequency range we have conducted shallow exploration using different methods, MASW, CCA of mini hexagon array, L-Shape SPAC, etc. using short period seismometers and geophones to cover the highest frequency range: from about 5 Hz to higher than 10 Hz.

Besides we filled the gap of dispersion curves appeared in some sites between 0.2 Hz and the lowest possible frequency of analysis by 2ST-SPAC around 0.3 Hz, by applying CCA to the records of scalene triangle arrays extracted from the irregular quadrilateral ones. However, the gap remained from 0.13 Hz to 0.2 Hz for all sites. We also filled other gaps at a few sites in higher frequency ranges, but lower than 1 Hz, using auxiliary the phase velocities calculated from zero crosses of the SPAC coefficient curves. Then, we applied the inversion of Vs structure from the determined dispersion curves. The estimated shear wave velocity structure showed a sharp Vs discontinuity at the depth of around 600 m and 400 m. According to a few deep drilling in KTV, it is interpreted that the former corresponds to the bottom of the basin, and it may be speculated that the latter a buried terrace.

Based on these observational activities we could show the efficiency and availability of irregular quadrilateral arrays and a comparison of various methods for shallow exploration.

Keywords: Microtremor Array Exploration; Irregular Shape Array; Deep Sediments; Kathmandu Valley

1. Introduction

Central Nepal was jolted by the 2015 Gorkha earthquake on April 25th (M_L 7.6, NSC/DMG; M_w 7.8 [6]). Its epicenter was determined about 80 km N-W from Kathmandu while the rupture was propagated eastward [7] passing through the Kathmandu Valley (KTV) which is filled of thick sedimentary layers [3]. The seismic intensity in the KTV was generally VI or VII of EMS-98 [8]. The strong motion records obtained at its central part show a significant amplification at around 0.25 Hz in the horizontal components [1], [2], [9], implying that exploration of shear wave velocity (V_s) structure of deep sedimentary layers is indispensable for a better seismic hazard assessment there.

The surface geology of the KTV consists of mainly three groups (Fig.1): the northern part consists of marginal fluvio-deltaic facies while the southern part consists mainly of alluvial fan facies and the central part consists mainly of lacustrine facies, caused by the rapid uplift of its southern rim that dammed the proto-Bagmati River and created a paleo-Kathmandu lake about one million years ago, where infilling process took place with a thick semi-consolidated Pliocene-Pleistocene fluvial and lacustrine sediments; its water-level lowered perhaps by earthquakes at around 48,000 and 38,000 years ago; finally drained 12,000 year ago. [3].

KTV has only few geophysical information for the deep structure. The gravity survey showed the existence of deep basin[10]. In 1988, the Kathmandu Valley Gas project drilled at Bhrikuti-Mandap, at its central part and a depth of non-weathered rock (green phyllite) at 570 m depth was reported (unpublished report of DMG, compiled by [11]). [12] gave a summary for studies of shallow structure before 2015.

Beside single point measurement for horizontal to vertical spectral ratio (HVSR) and shallow exploration, [11] conducted microtremor array measurement using acceleration sensors at five sites in its central part using equilateral triangular array for the deep sedimentary layers. A layer of V_s 600 m/s that they explored deepest, however, cannot be the seismic bedrock but the engineering bedrock. The deeper structure including the seismic bedrock depth has been left unrevealed.

Our research group: Group3-SATREPS started the activity in 2016. In the valley as a whole, the OYO Corp. team conducted the gravity survey [13], and the reflection survey Nov. 2018 at the Tribhuvan International Airport (TIA) and at the National Agriculture Research Institute (NARI). The deep structure is gradually getting revealed [15]. We conducted the exploration by deploying microtremor arrays at several sites using four sets of broadband seismographs (Fig.2) for estimating Vs structure of deep sediments from Dec. 2016 to May. 2019, in combination with shallow exploration.

Independently from SATREPS project, estimate of deep structure has been conducted, e.g., by [16], who detected a very low V_s structure at the USGS strong motion station down to the basement (V_s < 500 m/s to 470 m depth); [17] who determined V_s structures varies site by site and are consist of surface layers of very low V_s with a sharp contrast to the basement of which Vs is 3,200 m/s, except a bedrock sites; and [18] who performed microtremor array exploration using broadband seismometers at six sites in the valley and estimated the phase velocity up to about 800 m/s.

In this paper, we report the results of the microtremor exploration in a broad frequency range conducted in the framework of SATREPS in KTV, especially the availability of irregular shape arrays.

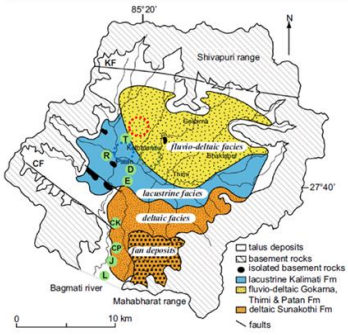

Fig. 1 Surface geology and geomorphology of Kathmandu Valley, after Sakai et al. (2016)[3].

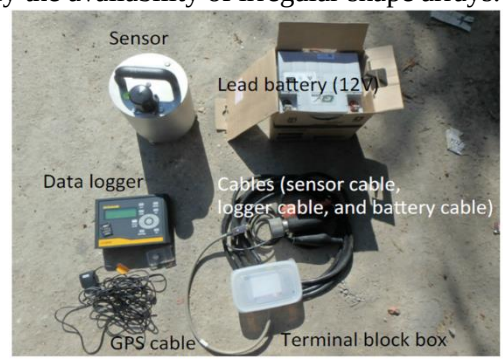

Fig. 2 Equipment used for microtremor exploration for deep sedimentary layers in Kathmandu Valley: CMG40T (Sensor) and LS8800 (Data Logger)

2. Methods

We applied the Spatial AutoCorrelation Method (SPAC) [19],[20],[21],[22], but especially the 2ST-SPAC[22] using irregular shape arrays for large scale in combination with of equilateral triangular ones for middle and small scales. We used auxiliary also the Centerless Circular Array method (CCA)[23] with scalene triangle arrays for large scale and equilateral triangular one for smaller ones. We deployed several arrays at same site to combine these dispersion curves. To grasp Vs of the most surficial layer we analyzed also the existing data of the L-shape SPAC (LS-SPAC)[24] and Multi-Channel Analysis of Surface Waves (MASW) [25] and conducted supplementary measurements for shallow exploration using MASW and CCA with mini-arrays of radius few meters in some sites to cover high frequency range. For filling the gap between the dispersion curves of large arrays and those of small ones we used zero-crosses of SPAC coefficient when necessary.

2.1 SPAC with regular and irregular shape arrays

SPAC is based on the following relation [19]. The SPAC coefficient:

$$\rho_{obs}(\omega,r) \equiv (1/2\pi)\int_0^{2\pi} Re\{C_{cx}(\omega,r,\theta)\}/C_{cc}(\omega,0,0)\,d\theta \cong (1/N)\sum_1^N \left[Re\{C_{cx}(\omega,r,\theta_n)\}/\sqrt{C_{cc}(\omega,0,0)\cdot C_{xx}(\omega,r,\theta_n)}\right] \quad (1)$$

is defined as the real part of the cross-spectra $C_{cx}(\omega,r,\theta)$ between two positions $c(r=0,\ \theta=0)$ and $x(r,\theta)$, normalized by the power spectra at $c(0,0)$. This $\rho_{obs}(\omega,\ r)$ becomes $J_0(\omega r/c(\omega))$, i.e., the 0-th order Bessel function of the first kind with argument $\omega r/c(\omega)$, where $c(\omega)$ the phase velocity of Rayleigh waves, and ω angular frequency[19]. The third member of Eq. (1) shows the practical way of calculation from field data. This formula of sum of coherence function over the discrete azimuth θ_n can suppress the influence of very local amplification and extract the contribution of laterally propagating surface waves [26]. Equilateral triangular arrays optimize the approximation of the integral over azimuth with the summation over the discrete azimuths [27], whereas [28] showed theoretical insight about the possibility of irregular shape arrays when the coherence function is only weakly or not dependent on the azimuth, that has been reported in a significant number of articles. [22] showed successful examples of real observation, where the coherence of individual station pairs without average over the azimuth played the role of the SPAC coefficient. They called their approach the 2ST-SPAC, because of its field application skipping the azimuthal average, and of the way to determine the dispersion curve by fitting to $J_0(\omega r/c(\omega))$ same as the SPAC.

In this study, we first confirmed the approximately isotropic (non-azimuth dependent) nature of the coherence functions in the low frequency range using equilateral triangle arrays at a site, then applied 2ST-SPAC to large trapezium arrays deployed at others, whereas for shallow exploration equilateral triangle ones.

2.2 CCA with scalene triangle array

CCA stands for the Fourier Transform of microtremor wave field over the azimuth [23]. The CCA coefficient $s_{obs}(\omega,r)$ is given by the spectral ratio of the power of the zero order Fourier Coefficient over the azimuth to that of the first order as follows.

$$s_{obs}(\omega,r) \equiv PSD\langle\int_{-\pi}^{\pi} Z(t,r,\theta)\,d\theta\rangle \Big/ PSD\langle\int_{-\pi}^{\pi} Z(t,r,\theta)e^{-j\theta}\,d\theta\rangle \cong \sum_{i=1}^{M}\sum_{k=1}^{M} C_{ik}(\omega,r) \Big/ \sum_{i=1}^{M}\sum_{k=1}^{M} C_{ik}(\omega,r)\,e^{-j(\theta_i-\theta_k)}, \quad (2)$$

where $PSD\langle\ \rangle$ denotes the power spectral density, $Z(t,r,\theta)$ time series of vertical component of microtremor at (t,r,θ), r,θ the radius of circular array and the azimuth from the center of the array to an observation point (station) on the peripheral circle. This $s_{obs}(\omega,r)$ is expected to converge to the known function $\{J_0(\omega r/c(\omega))/J_1(\omega r/c(\omega))\}^2$, where $J_1(\ )$ denotes the first order Bessel function of the first kind. The third member of Eq. (2) shows the practical way of calculation in the frequency domain from field data used in this study[25]. $C_{ik}(\omega,r)$ denotes the cross-spectra of the records obtained at the *i*-th and the *k*-th stations on the peripheral circle. The originally proposed array patterns are regular polygon such as equilateral triangles. Using the coherence in place of the cross-spectra in Eq. (2) can be a correction of very local amplification [26] and soften the requirement for irregular shape array expecting the semi-isotropic nature of the coherence. Therefore, for large size ones in this study we used arrays of 3 stations on the same circle but with un-even

azimuthal distribution. We avoided to use extremely acute-angled scalene triangle arrays. For all small scale cases, we used equilateral triangle ones.

3. Field Data Acquisition

We used 4 sets of the broadband seismometer CMG40T shown in Fig.2 for deep exploration using microtremor and the temporal continuous observation. For shallow exploration 7 short period seismometers (2 Hz, L22D, Sercel), 24 land geophones (4.5 Hz, GS11D, GEOSPACE) and 24 channels data logger McSeis/SW (OYO Corp.). Fig.3 shows the measurement sites' distribution in KTV.

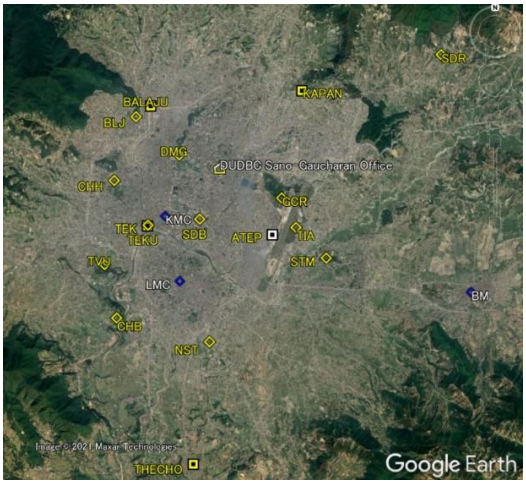

Fig.3 KTV: Sites of microtremor measurement and temporal seismic stations. (after Google Earth®)

Due to the densely built-up condition in cities, it was impossible to deploy equilateral triangle array of large scale except in SDB where a high security at roadside was confirmed (Fig.4a, b), and we had to use arrays of irregular shapes in others, of which maximum lateral extent reached to 1,400 m. The duration of recording for large arrays was basically one night for every deployment. Therefore, we selected locations in premises with guards. We deployed three large arrays in SDB and DMG, and two arrays in TEK whereas only one in others due to the limitation of time. For middle and small scale ones the recording duration was few hours or shorter.

4. Data and Analysis

We set the target frequency range from 0.02 Hz to 10 Hz. Using microtremor we could not determine the dispersion curves below 0.2 Hz at any site. We, therefore, complemented the lowest frequency range (0.01-0.13 Hz) with the phase velocity estimated using surface wave parts of tele-seismic records at 4 temporally fixed stations for continuous measurement [5] (hereafter denoted BDR). On the other hand, using MASW or LS-SPAC results we determined the phase velocity up to the 20 or 40 Hz, but we set the upper limit for further analysis at 10 Hz considering on the engineering interest. Using cubic spline interpolation [29] we resampled the phase velocity data obtained by different methods at regular intervals on the logarithmic axis. Then, we smoothed them using 7 points moving average filter. The outputs are denoted "Determined" in figures shown below.

4.1 Isotropic Nature of Coherence Function at SDB (Singhadurbar).

We checked the azimuthal dependency of the coherence function in Eq. (1) at **SDB** using the records obtained by two equilateral triangle arrays (S- and M-, Fig.4a). They gave approximately isotropic coherence functions for three different interstation distances (Fig.4b) and supported to use 2ST-SPAC for large scale

Fig.4a SDB (Singhadurbar): Configuration of Arrays deployed (after Google Earth®). Solid yellow segment denotes 500 m.

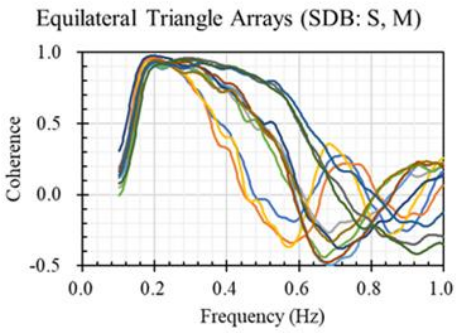

Fig. 4b SDB (Singhadurbar): Coherence functions of two equilateral triangular arrays (S- and M-Arrays).

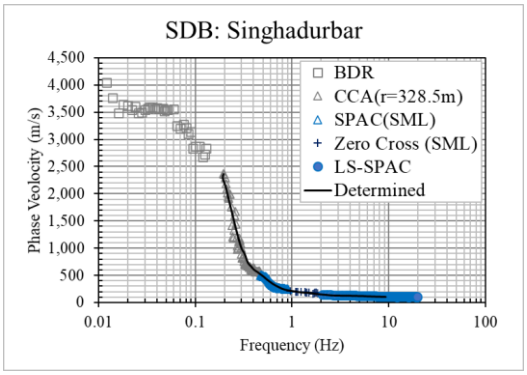

Fig.4c SDB (Singhadurbar): Determined dispersion curve.

Fig.5a TIA (Tribhuvan International Airport): Configuration of Arrays deployed (after Google Earth®). Solid yellow segment denotes 500 m.

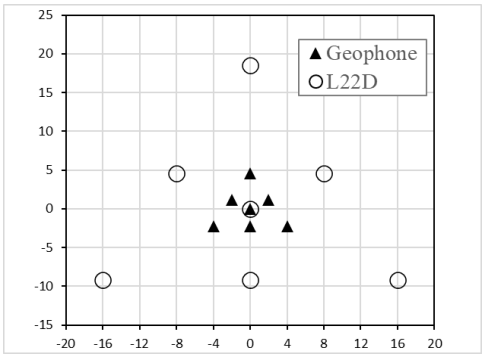

Fig.5b Nested array of small scale composed of 7 L22Ds (Open Circle: T-array) and 7 land geophones (Solid Triangle: P-array) recorded by McSeis/SW.

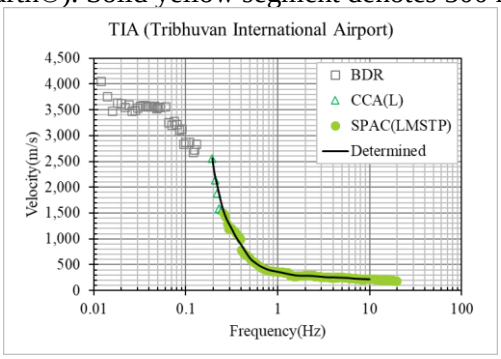

Fig.5c TIA (Tribhuvan International Airport): Determined dispersion curve.

arrays in KTV. A strong decay at about 0.2 Hz was observed at all sites. At this frequency the power spectra of microtremor were close to NLNM and suggested that the cause may be insufficient microtremor's power.

Then, in combination with S- and M- arrays we applied 2ST-SPAC using the large trapezium array, of which longest interstation distance is 829 m (Fig.4b). This covered the frequency range from 0.47 Hz to 0.9 Hz. We reanalyzed the existing LS-SPAC records [11] and covered from 2 Hz to 20 Hz. We filled the gap between 0.2 Hz and 0.47 Hz with those of CCA using a large scalene triangle array composed of 3 among 4 stations of L-array as shown by a circle of radius 329 m (Fig.4b), and the gap between 0.9 Hz and 2Hz using the phase velocities calculated from the zero-crosses of the oscillating part of the SPAC coefficients of mentioned S-, M- and L- arrays as shown in Fig.4c.

We have set a standard way, i) 2ST-SPAC using a large trapezium array together with equilateral middle and small scale arrays, ii) CCA using a large scalene triangle array to cover the gap at low frequency from 0.2 Hz, iii) extension of dispersion curve of 2ST-SPAC using the zero crosses of the SPAC coefficient curve or alternatives to fill the gap between 2ST-SPAC and shallow exploration, iv) LS-SPAC, CCA with mini array, and MASW, etc. were tested for shallow exploration to cover from few Hz to 10 or 20 Hz..

4.2 Nested Arrays at TIA (Tribhuvan International Airport)

We tested small scale equilateral triangular arrays using L22D and land geophones for iii) and iv) at **TIA**, where the reflection survey was performed [15]. We used 4 equilateral triangular arrays of the side length 8 m (land geophones, P-array), 32 m (L22D, T-array), 30 m (S-array) and 170 m (M-array) using CMG40T and combined them with a large trapezium one (L-array) with the longest interstation distance 948 m, as shown in Fig.5a, b. We conducted one day field work and one night recording for L-array, i.e., much shorter than SDB case, owing to the open space sufficiently wider for M-array. We applied 2ST-SPAC to the combination of these five arrays (LMSTP) and obtained a smooth dispersion curve (Fig.5c). We had to fill the gap between BDR and SPAC (LMSTP), i.e., from 0.2 Hz to 0.26 Hz with the results of CCA application to 3 among 4 stations of L-array that compose a circle of radius 474 m (Yellow broken circle in Fig.5a).

Fig.6a NST (National Academy of S & T): Configuration of Arrays deployed (after Google Earth®). Solid yellow segment denotes 500 m.

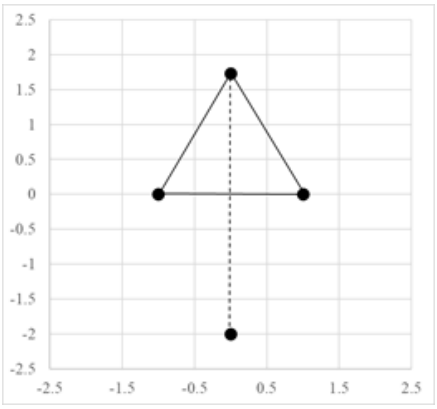

Fig.6b Mini umbrella array of side length 2 m used in NST.

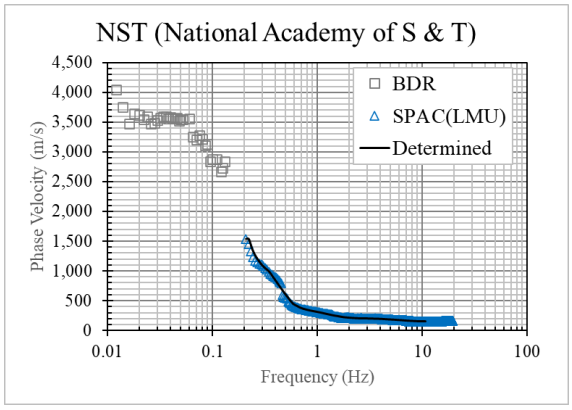

Fig.6c NST (National Academy of S & T): Determined dispersion curve and the results of analysis.

4.3 Mini Umbrella Array at NST (National Academy of Science and Technology)

Another way of shallow exploration was conducted at **NST.** In its premises we deployed an equilateral triangular array of side length 90 m (M-array), and a mini umbrella shape array [14] (U-array), all using 4 sets of CMG40T Fig.6a, b). We conducted one day field work at NST and one night recording for L-array as well as TIA. The U-array is composed of an equilateral triangle of the side length 2 m and one more seismograph located at a distance of 4 m from a vertex at opposite side (Fig.6b). We deployed also a large trapezium array (L-array) with the longest interstation distance 967 m (Fig.6a). Two stations at the west side of L-array were located in National Agronomical Research Institute, where a branch of reflection survey line was deployed [15]. We applied 2ST-SPAC to these 3 arrays in a combined way to determine the continuous dispersion curve owes to M-array that connects much bigger L-array to the mini array (Fig.6c).

4.4 Mini Hexagon Array at CHH (Chhauni Army Barrack – Hospital)

A hexagon array of 7 L22Ds were employed for iv) at **CHH,** located at the south of Swayambhu Nath. We deployed a large trapezium array with the longest interstation distance 876.6 m (SPAC(L), Fig 7a), and a mini hexagon array of radius 2 m. We filled the gap between these two arrays with the phase velocities calculated from the zero-crosses of the oscillating part of SPAC(L), whereas the gap between SPAC (L) and

Fig.7a CHH (Chhauni Army Barrack – Hospital): Configuration of deployed arrays (after Google Earth®). Solid yellow segment denotes 1,000 m.

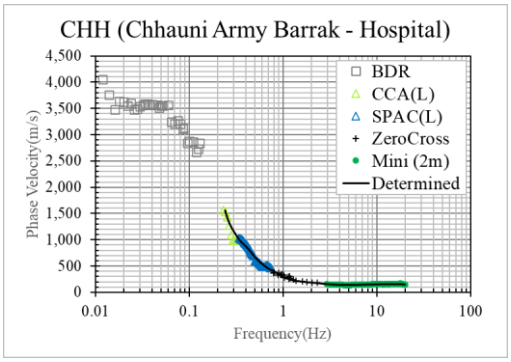

Fig.7b CHH (Chhauni Army Barrack – Hospital): Determined dispersion curve.

Fig.8a TVU (Tribhuvan University at Kirtipur): Configuration of Arrays deployed (after Google Earth®). Solid yellow segment denotes 1,000 m.

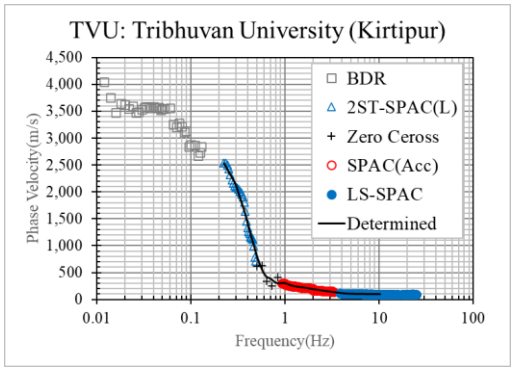

Fig.8b TVU (Tribhuvan University at Kirtipur): Determined dispersion curve and the results of analysis.

Fig.9a STM (Sano-Thimi): Configuration of deployed array. (after Google Earth®). Solid yellow segment denotes 500 m.

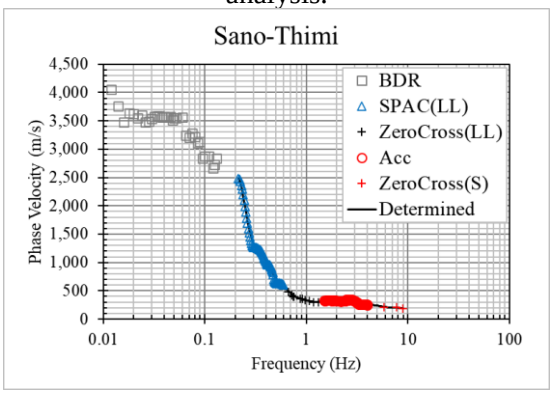

Fig.9b STM (Sano-Thimi): Determined dispersion curve.

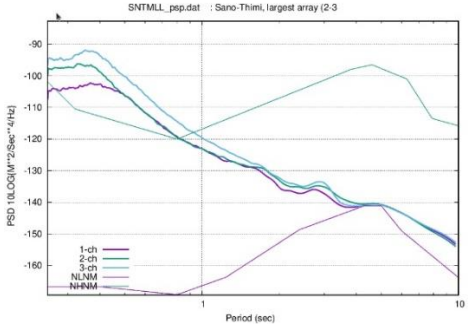

Fig.9c Power Spectral Density of the largest array (CMG40T) at STM with NHNM and NLNM

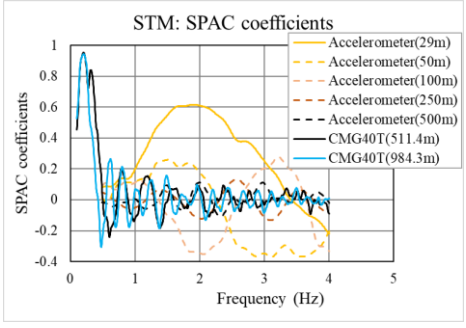

Fig.9d SPAC coefficients at STM

BDR with the results of CCA analysis using 3 seismographs of L-array, that are indicated by a big circle of radius 388.7 m (CCA(L), Fig.7a, b). In the small window in Fig.7a the locations of the mini hexagon array are shown. We used the mini hexagon array at DMG and TEK, too.

4.5 Combination with the Existing Acceleration Records of Microtremor

Examples of the combination with the existing acceleration records of microtremor were **TVU** (Tribhuvan University at Kirtipur) and **STM** (Sano-Thimi: National Examination Board). For **TVU**, we reanalyzed the existing LS-SPAC records for iv) and microtremor's acceleration records acquired using three equilateral triangular arrays [11]. Besides we deployed a large trapezium array to cover the frequency range lower than 1 Hz (Fig. 8a). A gap remained between 0.5 and 0.9 Hz was filled using the zero cross of their SPAC coefficients (Fig. 8b). For **STM**, we analyzed a large scalene triangular array for 2ST-SPAC (SPAC(LL), Fig.9a), because the fourth seismograph could not work properly. The dispersion curve of

Fig.10a TEK (Teku-Kalimati): Configuration of deployed arrays (after Google Earth®). Solid yellow segment denotes 1,000 m.

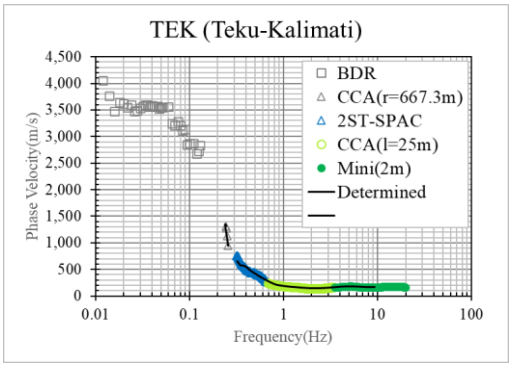

Fig.10b TEK (Teku-Kalimati): Determined dispersion curve.

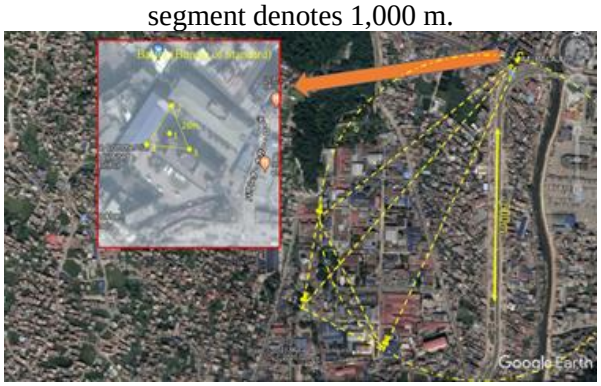

Fig11a BLJ (Balaju Industrial District): Configuration of deployed arrays (after Google Earth®). Solid yellow segment denotes 500 m.

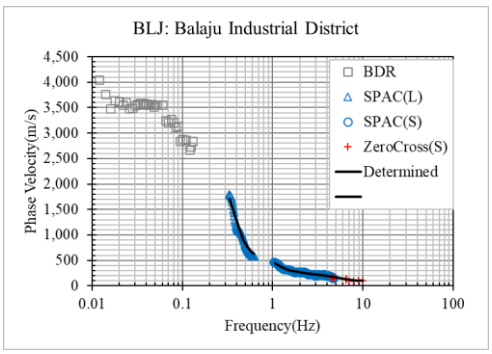

Fig.11b BLJ (Balaju Industrial District): Determined dispersion curve.

SPAC (LL) reached to 0.2 Hz. However, the gaps were remained around 1 Hz and higher than 4 Hz due to the limitation of acceleration data (Fig.9b, c, d). We filled it using the phase velocities calculated from zero crosses of SPAC coefficients of the largest array of acceleration measurement (Fig.9b).

4.6 On the Sag of SPAC Coefficients and Phase Velocity Observed Clearly

At some sites a slight disturbance of SPAC coefficient and therefore dispersion curves were observed at from 0.2 Hz to 0.3 Hz roughly as already reported for TEK case [30]. Except the sites **TEK** and **BLJ**, its influence was limited or can be made non-remarkable by applying interpolation and smoothing of dispersion curves.

In **TEK** (Teku Gas Well– Kalimati), we applied 2ST-SPAC to a scalene triangle array and a trapezium array shown in Fig.10a. The longest interstation distance is 1311.7 m. Also, CCA to large scalene triangle shown by a circle of radius 667.3 m. Besides we deployed a small equilateral triangle array of CMG40T with side length 25 m at Teku Gas Well of DMG (shown in a small window in Fig.10a, CCA(l=25m)). The highest frequency range is covered by the mini-array of radius 2 m for CCA, denoted "Mini (2m)" in Fig.10b. A sharp sag appeared in dispersion curve at around 0.3 Hz, that is caused by a sags of coherence functions. We had to make a clearance consciously to make smoothing possible (Fig.10b). A similar phenomenon took place at **BLJ** (Balaju Industrial District-Bureau of Standard). Its northern most station is also used for the continuous microtremor – earthquake observation for several months (Fig.11a). The longest interstation distance of the largest trapezium array (SPAC(L)) was 943 m among analyzed. Unfortunately, the power spectral density of one of these three includes several sharp peaks that are not in other two. The coherence functions have significant sags at their frequency. Therefore, again we had to make clearances consciously from 0.1 Hz to 0.3 Hz and from 0.6 Hz to 1 Hz to perform possible interpolation well (Fig.11b). Besides we deployed a small equilateral triangle array of CMG40T with side length 28 m in Bureau of Standard. This array (SPAC(S)) covers from 1 Hz to 4.5 Hz. The higher frequency range is filled by the data of phase velocity calculated from zero crosses of SPAC(S). These should be replaced with the real data of shallow exploration in future.

Fig.12a DMG (DMG-Narayanhiti): Configuration of deployed arrays (after Google Earth®). Solid yellow segment denotes 1,000 m.

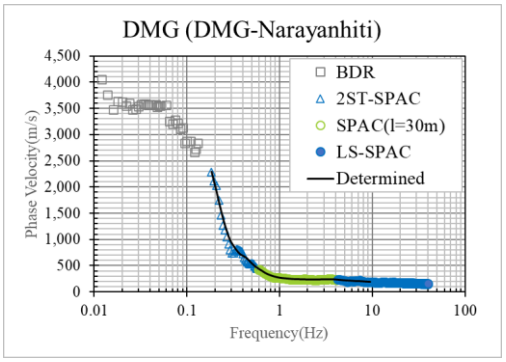

Fig.12b DMG (DMG-Narayanhiti): Determined dispersion curve and the results of analysis.

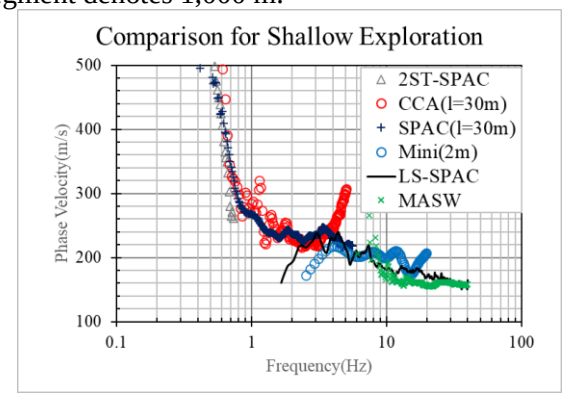

Fig.12c Comparison of dispersion curves of 4 types of small and mini arrays in DMG.

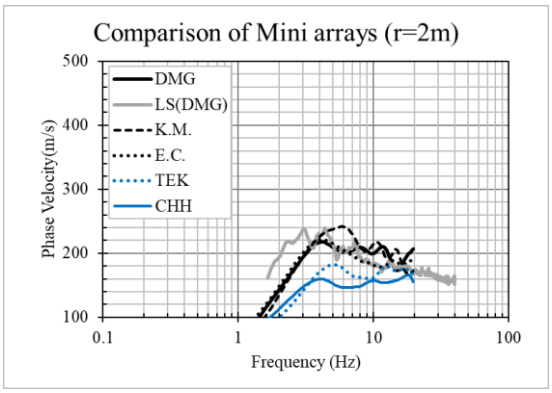

Fig.12d Comparison of dispersion curves obtained using mini array (2m) in KTV.

4.7 Comparison of Shallow Exploration methods at DMG

DMG (Dept. Mines and Geology - Narayanhiti Royal Palace Museum) provides an example of radial arrays. We deployed radial arrays from DMG premises across the Narayanhiti Royal Palace Museum (Fig.12a). The longest interstation distance is 1272 m. Also we applied SPAC to an equilateral triangle array of side length l=30 m using CMG40T in the DMG premises (denoted "SPAC (l-30m)" shown in a small window in Fig. 12a). Combining them with the existing LS-SPAC records [11], we determined the dispersion curve (Fig.12b). Besides we performed a mini regular hexagon array of radius 2 m for CCA using 2 Hz seismometers to compare with the phase velocity derived from the existing records of MASW and LS-SPAC for validation of different shallow exploration methods (Fig.12c). They were performed not exactly at the same positions and discrepancy at high frequency range may owe to the lateral variation of Vs structure. Fig.12d shows a comparison with other mini arrays in KTV. Close to the strong motion observation site of USGS (KANTP) [9], K.M. (Kaiser Mahal, 250 m) and E.C. (Premises of Election Commission, 150 m) are located, whereas DMG located at around 750 m (Fig.12d).

4.8 Exploration on the bedrock and at shallow sites.

Outcrops of bedrock have been reported in several places in KTV, for example, Kirtipur, Chobar, Pashupathinath etc. We conducted exploration in CHB (Chobar) where limestone is observed at the ground surface using an umbrella array of large scale (Fig.13a). The determined dispersion curve shows a flat part around 1,700-1,800 m/s in the frequency range from 2 Hz to 10 Hz and grows toward the lower frequency (Fig.13c). SDR is located at the foot of the mountain surrounding KTV in the northeast and expected to have a shallow sediment. We deployed a nested array (Fig. 5b) and an equilateral triangle array of side length 80 m. Its dispersion curve grows toward lower frequency from the flat part of 300 m/s at the frequency higher than 3 Hz and reaches to 1,500 m/s at 2 Hz. GCR (Gaucharan) is located close to an outcrop of bedrock at Pashupathinath. The dispersion curve is flat with 300 m/s at the frequency higher than 2 Hz. However, due to the lack of the microtremor power, the phase velocity at the frequency below 1 Hz could not be estimated.

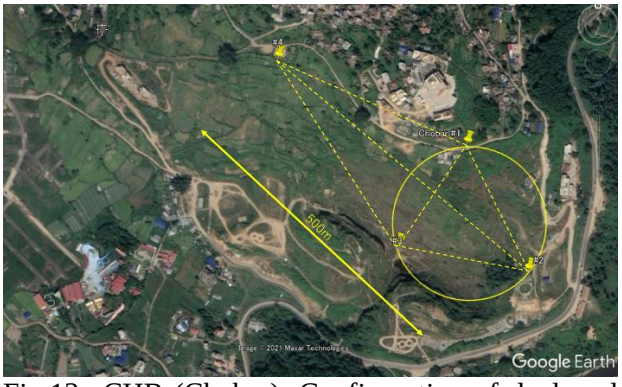

Fig.13a CHB (Chobar): Configuration of deployed arrays (after Google Earth®). Solid yellow segment denotes 500 m.

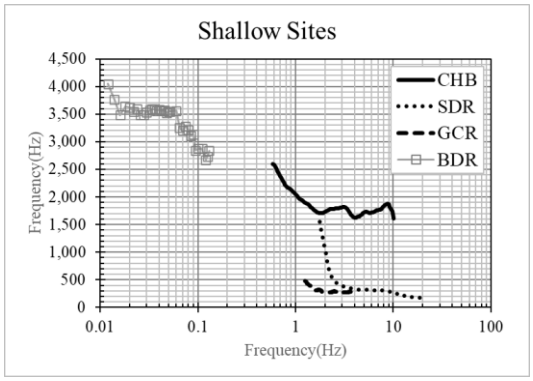

Fig.13b CHB (Chobar), SDR (Sundrijal), GCR (Gaucharan): Determined dispersion curves.

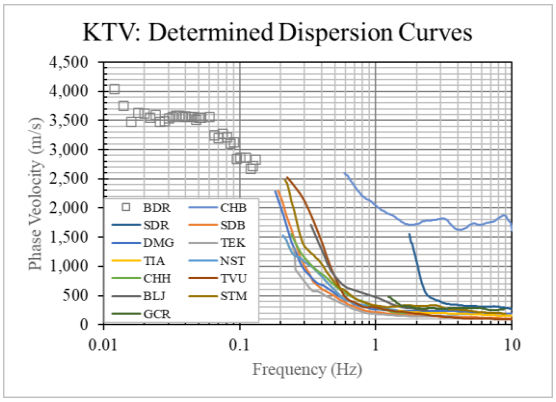

Fig.14a Summary of Dispersion curves in KTV.

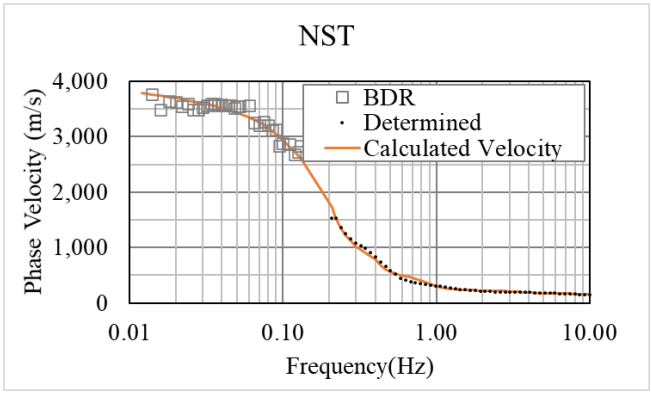

Fig.14b Example of fitting by inversion: NST

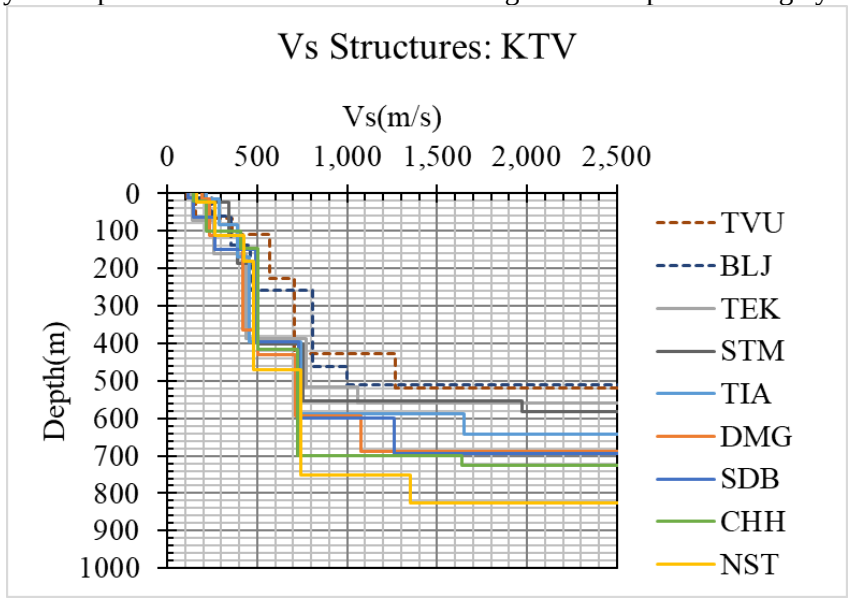

Fig.14c Inverted Vs structures at the central part of KTV.

4.8 Inversion from dispersion curve to Vs structure.

We resampled the combined dispersion curves into "Determined" ones as explained above (Fig.14a) and conducted the inversion by the combination of Down Hill Simplex Algorithm with Very Fast Simulated Annealing Method [29], [31] to obtain Vs structure from the dispersion curve. Fig.14b shows an example of comparison of the phase velocity data used as the input and calculated dispersion curve from the output Vs structure at NST. Fig.14c shows the inverted Vs structures except three shallow sites in Fig.13b.

5. Discussions and Conclusion

The borehole of Bhrikuti-Mandap between KMC and SDB in Fig.3 has the depth of non-weathered rock at 570 m depth. This may correspond to a concentration of Vs discontinuities of SDB, DMG and TIA at around the depth 600 m with Vs from 700 to 1,200 m/s. (Fig.14c). This is shown shallower for TEK and STM, whereas at CHH estimated much deeper and at NST the deepest. Another concentration of curves except the broken ones is obvious in Fig.14c at the depth around 400 m to 450 m with Vs from 500 to 700 m/s. This can be just speculated as a buried terrace formed during drained period of the Paleo-Kathmandu lake [3], and below NST and CHH a paleo-gorge between terraces. Different pattern of structure is estimated for TVU and BLJ. The former is close to the buried cliff at Chobar, and the latter close to the boundary between hilly terrain and plain. We have been able to vaguely imagine the three-dimensional underground Vs structure of KTV. Combined analysis with the gravity survey will be given in 17WCEE [32].

As an accommodation with severe reality in the field works, irregular quadrilateral arrays for deep exploration were tested and evaluated available and useful, although the processing was somewhat skillful in comparison with regular shape arrays. Besides we performed shallow exploration using mini-umbrella array, LS-SPAC, nested array, mini hexagon array for CCA. All of them worked well and gave acceptably comparable results. We can select some of them and use properly according to the situation at each site.

7. Acknowledgements

This study was supported by Japan Science and Technology Agency and Japan International Cooperation Agency (JICA) under the “Science and Technology Research Partnership for Sustainable Development (SATREPS): Integrated Research on Great Earthquakes and Disaster Mitigation in Nepal Himalaya (FY2016-2021)”. We greatly thank also to JICA, Oriental Consultants Global Co. Ltd. & OYO International Corporation for providing us the data for LS-SPAC at SDB and DMG.
For data processing, we used the following software that one of the authors (TY) opens in public.
SPAC: https://iisee.kenken.go.jp/net/?mod=spac
CCA: https://iisee.kenken.go.jp/net/?mod=cca
MASW: https://iisee.kenken.go.jp/net/?mod=masw

8. REFERENCES

[1] Bhattarai M, Adhikari LB, Gautam UP, Laurendeu A, Labonne C, Hoste- Colomer R, Sebe O, Hernandez B (2015): Overview of the large April 25th Gorkha, Nepal earthquake from accelerometric prospective, *Seism. Res. Let.*, 86, 40-48.
[2] Takai N, Shigefuji M, Rajaure S, Bijukchhen SM, Ichiyanagi S, Dhital MR, & Sasatani T (2016): Strong Ground Motion in the Kathmandu Valley during the 2015 Gorkha, Nepal, Earthquake, *Earth Planets and Space*, 68(10),1-8.
[3] Sakai H, Fujii R, Sugimoto M, Setoguchi R & Paudel MR (2016): Two times lowering of lake water at around 48 and 38 ka, caused by possible earthquakes, recorded in the Paleo-Kathmandu lake, central Nepal Himalaya, *Earth Planets and Space*, 68, 31, 1-10.
[4] Yokoi T, Hayashida T, Bhattarai M, Pokharel T, Shresta S, Timsina Ch, Bhattarai S, Nepali D (2019): Broadband Microtremor Array Exploration at and around Tribhuvan International Airport, Kathmandu, Nepal, SSS13-P33, *Proceedings of JPGU2019*, Tokyo.
[5] Hayashida, T, Yokoi, T, Bhattarai, M (2018): Phase velocity of long-period surface waves in the Kathmandu Valley, Nepal, inferred from continuous broadband seismic data, *Proceedings of SSJ Fall Meeting*.
[6] United States Geological Survey (2015a): *https://earthquake.usgs.gov/earthquakes/eventpage/us20002926#executive* . Accessed Jan. 27, 2021.
[7] Koketsu K, Miyake H, Kobayashi H, Masuda T, Davuluri S, Bhattarai M, Adhikara LB, & Sapkota SN (2016): Widespread ground motion distribution caused by rupture directivity during the 2015 Gorkha, Nepal earthquake, *Scientific reports*, 6 (1), 1-9.
[8] Martin SS, Hough SE, Bilham R & Hung C (2015): Ground motions from the 2015 Mw 7.8 Gorkha Nepal, Earthquake, constrained by the detailed assessment of Macro seismic data, *Seism. Res. Lett*., 86(6), 1524-1532.
[9] United States Geological Survey (2015b): Net Quakes Station KATNP_NQ_01, 25 April 2015, *http://earthquake.usgs.gov/monitoring/netquakes/station/KATNP_NQ_01/20150425061138/*. Accessed Jan. 27, 2021

[10] Moribayashi S & Maruo Y (1980): Basement Topography of the Kathmandu valley, Nepal- An application of gravitational method of the survey of the tectonic basin in the Himalayas, *Jour. Japan Soc. Eng. Geol.*, 21(2), 30-37.
[11] JICA (2018): *The Project for Assessment Of Earthquake Disaster Risk For The Kathmandu Valley In Nepal (Final Report), Vol. 2 Main report*, Japan International Co-operation Agency and Ministry of Home Affairs of Nepal.
[12] Molnar S, Onwuemeka J, & Adhikari SR (2018): Rapid Post-Earthquake Microtremor Measurements for Site Amplification and Shear Wave Velocity Profiling in Kathmandu, Nepal, *Earthquake Spectra*, 33, S1, S55–S72
[13] Shrestha S., Pradhan O., Shimoyama M., Koshika K., Kobayashi K., Dhakal S., Komazawa M., Nozaki K., Nepali D., Sapkota S. M., Matsuyama M., Miyake H., Koketsu K., (2021): Gravity Survey in Kathmandu Valley, Nepal for the Estimation of Basement Structure, submitted to 17WCEE.
[14] Yamada M., Cho I., Kuo C.-H., Lin C.-M., Miyakoshi K., Guo Y., Hayashida T., Matsumoto Y., Mori J., Yen Y.-T., Kuo K.-C. (2020): Shallow Subsurface Structure in the Hualien Basin and Relevance to the Damage Pattern and Fault Rupture during the 2018Hualien Earthquake, Bull. Seism. Soc. Am., 110, 2939-2952, doi:10.1785/0120200063.
[15] Kawasaki Y., Koshika K.,Pradhan O., Kurosawa H., Abe K., Yamamoto M., Nobuoka D., Matsubara Y., Jha M., Timsina C., Shrestha S., Pokharel P., Nepali D., Bhattarai M., Sapkota S.N., Matsuyama H., Miyake H., Koketsu K., (2019):Subsurface Structure of the Kathmandu Valley Revealed by Seismic Reflection and Gravity Surveys, T33E-0370, AGU Fall Meeting, San Francisco CA.
[16] Dhakal YP, Kubo H, Suzuki W, Kunugi T, Aoi S & Fujiwara H (2016): Analysis of strong ground motions and site effects at Kantipath, Kathmandu, from 2015 Mw 7.8 Gorkha, Nepal earthquake and its aftershocks, *Earth, Planets and Space*, 68(1), 1-12.
[17] Bijukchhen S, Takai N, Shigefuji M, Ichiyanagi M, Sasatani T. & Sugimura Y. (2017): Estimation of 1-D velocity models beneath the strong motion sites in the Kathmandu Valley using strong motion records from moderate-sized earthquakes, *Earth, Planets and Space*, 69(1), 1-16.
[18] Poovarodom N, Chamlagain D, Jirasakjamroonsri A & Warnitchai P (2017): Site characteristics of the Kathmandu Valley from array microtremor observations, *Earthquake Spectra*, 33(1_suppl), 85-93.
[19] Aki K (1957): Space and time spectra of stationary stochastic waves, with special reference to microtremor, Bull. Earthquake Res. Inst. Tokyo Univ., 35, 415–456.
[20] Aki, K., 1965, A note on the use of microseisms in determining the shallow structures of the earth's crust, *Geophysics*, 30, 665–666.
[21] Okada H (2003): *The Microtremor Survey Method. Geophysical Monograph Series, no 12*, Society of Exploration Geophysics.
[22] Hayashi K, & Craig M (2017): S-wave velocity measurement and the effect of basin geometry on site response, east San Francisco Bay area, California, USA, Physics and Chemistry of the Earth, Parts A/B/C, 98, 49-61.
[23] Cho I, Tada T & Shinozaki Y (2014): A New Method to Determine Phase Velocities of Rayleigh Waves from Microseisms, *Geophysics*, 69, 1535-1551.
[24] Geometrics (2009): *SeisImager/SW™ Manual, Windows Software for Analysis of Surface Waves*, https://www.geometrics.com/ttps://www.geometrics.com/ . Accessed Jan. 19, 2021.
[25] Hayashi K & Suzuki H (2004): CMP cross-correlation analysis of multi-channel surface-wave data, *Exploration Geophysics*, 35, 7–13.
[26] Yokoi T (2014): On the Correction of System Characteristics and Improvement of the Long Wave Length Approximation for Microtremor Exploration Using Small Scale Array, BUTSURI-TANSA, 67, 255-266.
[27] Okada H (2006): Theory of efficient array observations of microtremors with special reference to the SPAC method, *Exp. Geophysics*, 37, 73-85.
[28] Shiraishi H, Matsuoka H & Asanuma H (2006): Direct estimation of the Rayleigh wave phase velocity in microtremor, *Geophys. Res. Lett.*, 33(18).
[29] Press WH, Teukolsky SA, Vetterling WT & Flannery BP (1996): *Numerical Recipes in Fortran 77 2nd Ed. Final version 2.10*, Cambridge University Press.
[30] Yokoi, T, Hayashida, T, Bhattarai, M, Pokharel, T, Dhakal, S, Shrestha, S, Timsina, C, Nepali, N (2018): Deep Exploration using Ambient Noise in Kathmandu Valley, Nepal - with an emphasis on CCA method using irregular shape Array-, Proceedings of the 13th SEGJ International Symposium, Tokyo.
[31] Yokoi T. (2005): Combination of Down Hill Simplex Algorithm with Very Fast Simulated Annealing Method - An effective Cooling Schedule for Inversion of surface wave's dispersion curve, Programme and Abstracts, the Seismological Society of Japan, Fall Meeting.
[32] Matsuyama H., Suzuki H., Pradhan O., Matsubara Y., Komazawa M., Nozaki K., Hiramatsu S., Timsina C., Shrestha S., Dhakal S., Nepali D., Bhattarai M., Sapkota S. N., Takai N., Shigefuji M., Yokoi T., Hayashida T., Miyake H., Koketsu K. (2021): Construction of Velocity Structure Model of The Kathmandu Basin for Strong Ground Motion Prediction, submitted to 17WCEE.

